A R C H I V E S O F M E T A L L U R G Y A N D M A T E R I A L S
Volume 60 2015 Issue 3
DOI: 10.1515/amm-2015-0368

J. MARCZAK*#

MICROMACHINING AND PATTERING IN MICRO/NANO SCALE ON MACROSCOPIC AREAS

MIKROOBRÓBKA I LITOGRAFIA W MIKRO- NANO- SKALI W OBSZARACH MAKROSKOPOWYCH

This paper presents detailed discussion of selected examples of laser technologies for the modification of solid surfaces, including topographic and microstructural changes as well as both these alterations simultaneously. Laser surface micromachining has just entered the new generation of technologies that are used in surface engineering. It will be shown on the examples of applications in bioengineering, on the base of the author's own research, in modification of materials such as titanium and its alloys, diamond-like layers (DLC) deposited on silicon and polymer substrates.

Keywords: lasers, surface modification, texturing, interference lithography, direct writing

Artykuł przedstawia szczegółowe omówienie wybranych przykładów technologii laserowych związanych z modyfikacją powierzchni ciał stałych, obejmujących zmiany topograficzne i zmiany mikrostrukturalne, lub obie te zmiany jednocześnie. Laserowa mikroobróbka powierzchni weszła już do nowej generacji technologii, wykorzystywanych w inżynierii powierzchni. Zostanie to pokazane, na podstawie prac własnych, na przykładach zastosowań w bioinżynierii, w modyfikacji takich materiałów jak tytan i jego stopy oraz warstwy diamentopodobne (DLC) naniesione na podłoże krzemowe i polimerowe.

1. Introduction

Starting from the date of laser invention [1], we are facing a never-ending interest in the practical use of lasers in all scientific domains, industry, medicine, and in the awaiting, still undiscovered applications. Such wide utilisation of laser radiation is directly connected with its uncommon properties. The high spatial coherence of laser radiation allows extreme orientation and concentration of photon flux, nowadays achieving a power density of over 10^{21} W/cm^2. Laser light monochromaticity, along with wavelength tuning, opens the next possibility of highly selective, narrowband excitation of different media. Controlled, pulse and selective material excitation offers in turn high temporal resolution (nano-, pico- and femtosecond pulses), which allows overcoming of the concurrent physical-chemical phenomena that occur sometimes simultaneously during the laser-matter interaction. The combination of all these properties offers wide and comprehensive application of lasers in domains which are totally different in terms of technology and field of study [2-6].

Laser machining is a noncontact technology, in which a focused laser beam is transferring a part of its energy to the treated material. On the machined surface of the material occurs the process of absorption and reflection of laser radiation. The amount of absorption plays an important role in the efficiency of the transfer of energy from the laser to the place of interaction. Locally absorbed energy leads to a controlled temperature rise, causing phase changes in the material (e.g. melting, evaporation). The final result of laser processing depends on laser beam parameters (energy density – fluence, wavelength and temporal parameters), on physical and chemical properties of treated material. It depends also on the condition of material surface. A particular application of the laser processing technology needs one or more of those wonderful laser light properties.

One of the main applications of laser radiation in materials engineering is the modification of surface properties [5]. Material surfaces can be modified in different ways to fulfil the specific physical, chemical and mechanical requirements. It includes technologies such as e.g. deposition [6], crystallisation, recasting, glazing, texturing or laser shock peening.

Generally, laser technology in material surface engineering includes processes shown in (Fig. 1). Thanks to them, it is possible to attain enhanced wear resistance, increase or reduction

* INSTITUTE OF OPTOELECTRONICS, MILITARY UNIVERSITY OF TECHNOLOGY, 2 GEN. SYLWESTRA KALISKIEGO STR., 00-908 WARSZAWA, POLAND
# Corresponding author: jan.marczak@wat.edu.pl

of surface reflection coefficient as well as many other properties that are useful, among others, in medicine [7] and bioengineering [8-10].

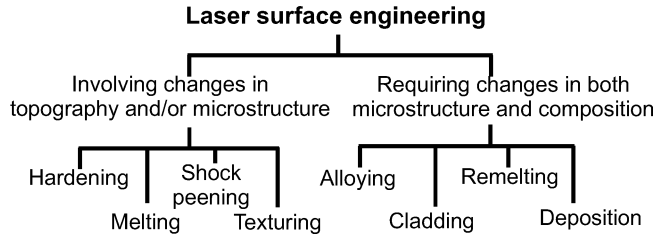

Fig. 1. General classification of technological processes with the use of lasers in surface engineering

Some surface properties need structure dimensions ranging from several to a few dozen micrometres, e.g. oil micro-trays, printing ink cells. For other applications, modified surfaces need structures with significantly smaller dimensions on the level of tens to hundreds of nanometres. As a consequence, a wide diversity of surface topography in different scales, with various properties and spatial distribution is needed.

Apart from the already common laser volumetric material processing (cutting, drilling, welding), lasers are utilised in micro and nanoprocessing, but particularly in **surface engineering** – which is a part of materials science. The surface engineering involves the processes of creating top surface layers and coatings as well as their modification (changes in surface topography and its micro-structuring), investigation of the accompanying phenomena as well as obtaining the final, exploitable results [11].

Processes of laser micro and nanoprocessing with utilisation of different types of lasers and various radiation parameters, tailored to the specific process, have already entered the new generation of technologies in surface engineering. Surface modification using laser radiation is conducted virtually on all kinds of materials: metals, semiconductors, dielectrics, ceramics, polymers, composites and even on gradient materials.

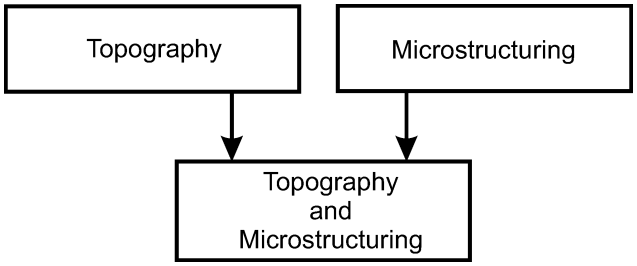

Fig. 2. Modulation of two main surface properties

The subject of this review are the selected examples of laser technologies connected to modification of surface of solids, including topographical or/and microstructural changes. Modulation of these two main properties of the surface of materials (Fig. 2) which are particularly useful in bioengineering, such as titanium and its alloys, diamond-like carbon layers (DLC) deposited on silicon and polymer substrates is presented in the following chapters of this review. The content is based on the results of a research conducted in the Group of Laser Applications at the IOE MUT in cooperation with the Institute of Metallurgy and Materials Science, Polish Academy of Sciences in Cracow.

2. Laser modification of material surface layers

Modification of the outer layers with the use of laser radiation can be performed below the ablation (etching) threshold of the target material, as well as above the ablation threshold. The term "ablation" in the literature means (from the Latin "ablatio") a set of complex physical-chemical processes, resulting in subtraction of a material layer from the surface (1) or the volume (2) of a solid. Today, this term describes also any laser supported process of material removal, including etching products as well as the emission of electrons and ions [12].

The first set of technologies (topographical changes) includes heating, hardening, polishing, recrystallisation, surface cleaning [13], material photoactivation [14] and many others. The second set of microstructuring technologies includes in general 1D-3D processes in which the target material is removed according to an earlier and precisely designed pattern.

In practice, laser power densities below the level of $10^{10} \div 10^{11}$ W/cm^2 are used in experiments conducted in normal atmospheric conditions, determining the ionisation threshold in dry air (laser spark). The emitted laser energy flux will not reach the target surface at higher power densities. Levels of air ionisation are the function of the emitted radiation wavelength, beam dimensions at the focus, duration of the laser pulse, and are dependent on air contamination and humidity. A typical, threshold value for clean air and a CO_2 laser (10.6 μm) with pulse duration above 1 μsec amounts to 10^9 W/cm^2. Air ionisation threshold increases with the decrease of laser pulse duration, reaching the value of 10^{10} W/cm^2 for a wavelength of 1.06 μm and pulse duration of 10^{-8} sec as well as around 10^{11} W/cm^2 for a pulse duration of 10^{-10} sec. Air ionisation threshold scales with the square of the wavelength in the infrared range of spectrum.

Laser micro/nano-processing needs precise distribution of the energy density across the laser beam. The precision and processing quality are also influenced by the wavelength, laser pulse duration, pulse repetition frequency, position of focal plane against the target, and depend on the physical-chemical properties of the processed material.

3. Surface modification methods in micro- and nanoscale

Modulation of the two main surface properties (Fig. 2) is mainly realised using the following methods:

1. Laser direct writing (LDW);
2. Mask projection (MP);
3. Direct laser interference lithography (DLIL);

4. Laser induced, self-organised periodic surface structures – "ripples" (LIPSS);
5. Combined techniques;
6. Scribing method.

The first five methods create basically "2½" dimensional structures utilised in fabrication of micro-fluidic systems or diffraction gratings in micro/nanoscale. The classical, completely three-dimensional technique is the sixth method, called "scribing", which can be compared to mechanical grinding.

All the abovementioned methods of surface modification are in practice based on the process of laser ablation or laser etching in the presence of gases, liquids or plasma [7,12]. The removal of materials with the use of pulse laser radiation has been called "laser ablation", as to differentiate this process from the vaporisation phenomenon, which occurs under thermodynamic equilibrium conditions. The ablation process is utilised precisely in the fabrication of holes, dimples, scratches, channels, masks, gratings and other 1D-3D patterns in micro- and submicro scales.

3.1. Laser direct writing

The technique of direct writing involves focusing a laser beam on the target surface, creating predefined points or lines in a continuous manner – cw lasers or quasi-continuous regime pulse, high repetition lasers [5,7,15]. Micromachining of a specified pattern is realised by the movement of substrate with respect to the fixed laser beam position, or by a motion of laser head with respect to the fixed target position (Fig. 3a). A faster method involves scanning with the focused laser beam with respect to the fixed target position (Fig. 3b), using a galvanometric scanner with telecentric F-Theta lens [16]. A combination of both methods, which is also sometimes used, expands the treatment area and allows deposition of patterns at larger surfaces.

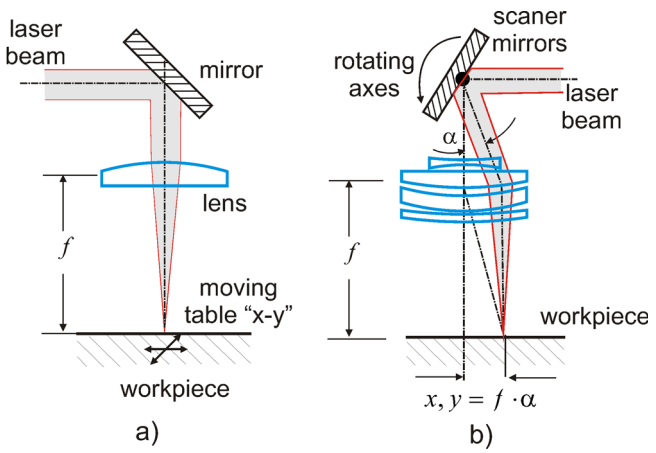

Fig. 3. Depiction of two fundamental techniques of direct writing: a) with the use of „x-y" tables; b) utilising a telecentric galvanometric scanner [16]

(Fig. 4) presents a diagram that illustrates the definition of overlapping of laser spots at the focusing plane of the converging lens. Laser beam overlapping is different, from point to quasi-continuous, depending on the desired pattern. As an example, precise fabrication of fluidic micro-channels needs the range of overlap between 75% and 95%.

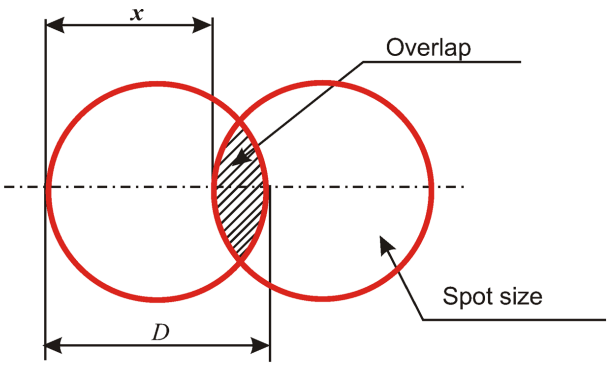

$$R_{overlap} = \frac{D - x}{D} \cdot 100\% \qquad x = \frac{\upsilon}{f}$$

where: υ *- scanning velocity, f - laser pulse repetition frquency*

Fig. 4. Depiction of overlapping of laser beams and definition of beam overlapping in the laser micromachining process

Both techniques of laser direct writing have been exploited during the fabrication of surface micro- and nanostructures, aimed at the observation of the behaviour of stem cells as well as in the prototyping of *"Lab On a Chip"* microfluidic systems.

3.1.1. Texturing of biocompatible material surfaces

The technique of direct writing has been implemented in the structuring of biocompatible material surfaces. Topographical response of cells and tissues to the pattern and form of structuring is one of the main issues in the design of structures and biomaterials. If the response of cells and tissues to the topographical substrate alterations is different, then this dependence can be utilised in:

- modulation of cell functions,
- design of implant materials,
- cell growth control,
- spatial cell orientation.

It has been shown during investigations that biomaterials preserving (transferring) the same form of mixed surface are able to control the cellular growth, which in a specified case is known as a contact-duplication direction.

(Fig. 5) shows a TiN layer deposited onto a silicon substrate, along with a so called "hierarchical structure" fabricated at its surface. The patterns have been created using the IVth harmonics (266 nm) of a picosecond (60 ps) diode pumped Nd:YAG laser. This structure was utilised as one of the templates in culturing of cells and their directional growth [17].

(Fig. 6) presents the examples of structuring of the DLC layers with the thickness of 200 nm, which were applied on a silicon wafer (diameter 65 mm) using pulse laser deposition

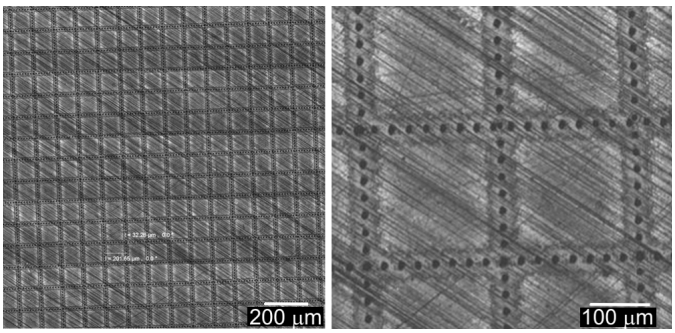

Fig. 5. A structure of "dimples" (diameter around 10 µm, depth 50 nm) in a 100 nm TiN layer, deposited using the PLD method on a silicon substrate (diameter 65 mm). Distance between dimples was around 30 µm [17]

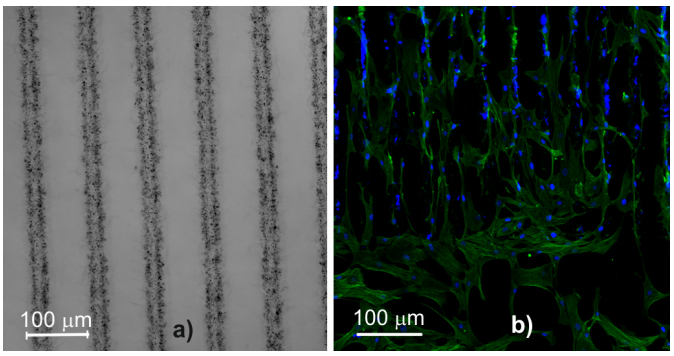

Fig. 7. Example of a linear structure of microchannels in glass (a) and directional growth of smooth muscle cells in the upper part (b)

(PLD) method. Directional and linear growth of smooth muscle cells outside the fabricated grooves is shown in figure 6b, whereas figure 6d shows clustering of cells around shallower dimples (upper row).

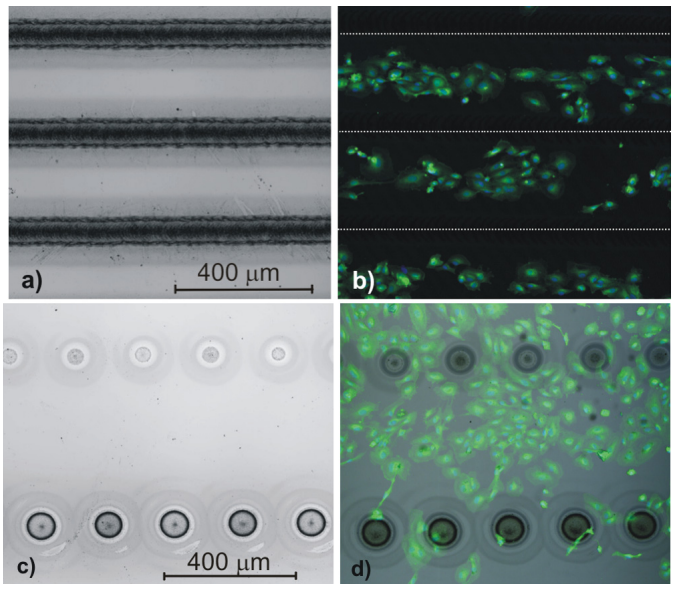

Fig. 6. Microphotographs of linear (a,b) and dot (c,d) structure of patterns created on a 200 nm thick DLC layer on a silicon substrate. Width of lines around 50 µm, depth 100 nm. Horizontal distance between dots around 200 mm, vertical distance between dots around 600 µm. Photographs c and d depict the development of smooth muscle cells

The next example of laser machining of linear structures and directional response of the development of smooth muscle cells, this time on a glass substrate, is shown in figure 7.

3.1.2. Fabrication of microfluidic "*Lab On a Chip*" devices

Design and manufacturing of the "*Lab On a Chip*" microfluidic systems allows, in a simplified description, chemical and biological experimentation in the microscale. PC and PMMA polymers, silicon and quartz glass are the most popular materials for fabrication of these structures. The typical area of microfluidic devices ranges from several mm^2 to several cm^2, providing a substantial decrease in the consumption of expensive samples and reagents ($10^{-6} \div 10^{-9}$ ml). Chemical reactions in microsystems occur in shorter time and require simplified procedures [18].

The direct writing technique plays a dominating role in the microfluidic technology due to its flexibility, and it is competitive in relation to the classical lithography. Direct laser writing allows fast prototyping of structures (in many cases disposable), taking into account the uniqueness of particular projects. Main inconveniences are represented by difficulties in the creation of a constant depth and the smooth surface of microchannels (Fig. 8). These characteristics in turn decrease the optical transparency and disturb the laminar flow of reagents, which is essential, among others, in the diffusive or electrophoretic microparticle separation systems [19].

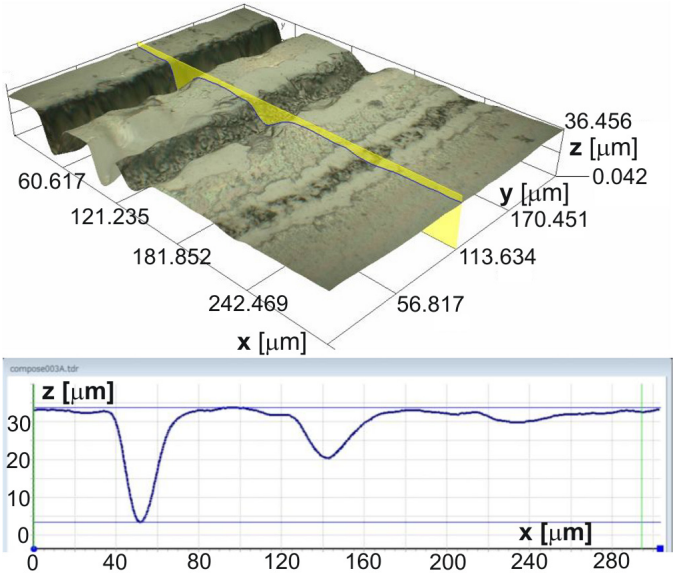

Fig. 8. 3D image and cross-section (Hirox digital optical microscope) showing in micrometric scale the structure of grooves with different depth and width, applied to fused quartz with the use of picosecond laser pulses (IIIrd harmonics – 355 nm, 60 ps) from Nd:YAG laser

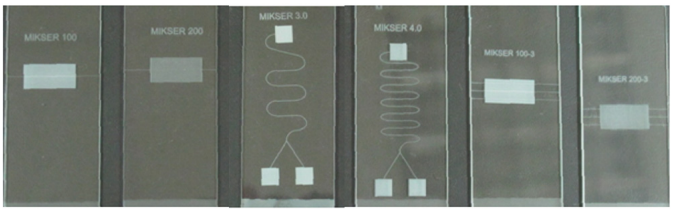

Fig. 9. Examples of mixers engraved into microscope slides and quartz using picosecond laser pulses (IIIrd harmonics – 355 nm, 60 ps, repetition 1 kHz) from Nd:YAG laser. Scanning velocity 2 – 10 mm/sec. Laser written sample inscriptions

3.1.3. Direct laser structuring of nanocellulose hydrogels

Small dimensions and heterogeneity of pores in the bacterial nanocellulose hydrogels (BNC) limit cellular growth and their application as cellular engineering materials for implants. Circumvention of this limitation can be based on the use of fillers during BNC biosynthesis or on the introduction of post-processing stages, like non-contact laser perforation. Homogeneous and functional nucleation needs three-dimensional ordering of channels. Figure 10 shows one-directional or three-dimensional perforation of BNC hydrogels using a CO_2 pulse laser. In comparison with non-modified BNC, the BNC perforated in one direction or three-dimensionally allows growth and migration of the primary animal/human cartilage cells through the network of BNC nanofibers. As a rule, perforated BNC is highly biocompatible and it provides short diffusion channels for the nutrients and the extracellular template components. The created microchannels support migration to the BNC and formation of the template. This can be utilised in "in vivo" applications, e.g. as a material substituting the cartilage [20].

3.2. Direct laser interference lithography

Direct laser interference lithography (DLIL) involves irradiation of virtually any solid surface with a proper interference pattern by means of high power density pulse laser (from MW/cm^2 up to GW/cm^2). DLIL is a technology recently used in medicine, surface bioengineering and tribology in order to obtain the desired surface topography and microstructure.

In practice, all biomedical implants are characterised by a limited lifetime. The number of appropriate treatments and processes intended to extend their lifetime or to improve biocompatibility therefore increases. These processes are also related to the additionally deposited adequately thin layers of different biocompatible materials and their modifications.

Particular attention during the last two decades was paid to titanium alloys (Ti6Al4V and Ti13Nb13Zr), as well as to amorphous carbon (DLC). The DLC is characterised by high smoothness, low friction coefficient, is chemically inert and abrasion-resistant. Its optical, mechanical, thermal and electrical properties are the function of manufacturing – mainly depending on its chemical composition [21,22].

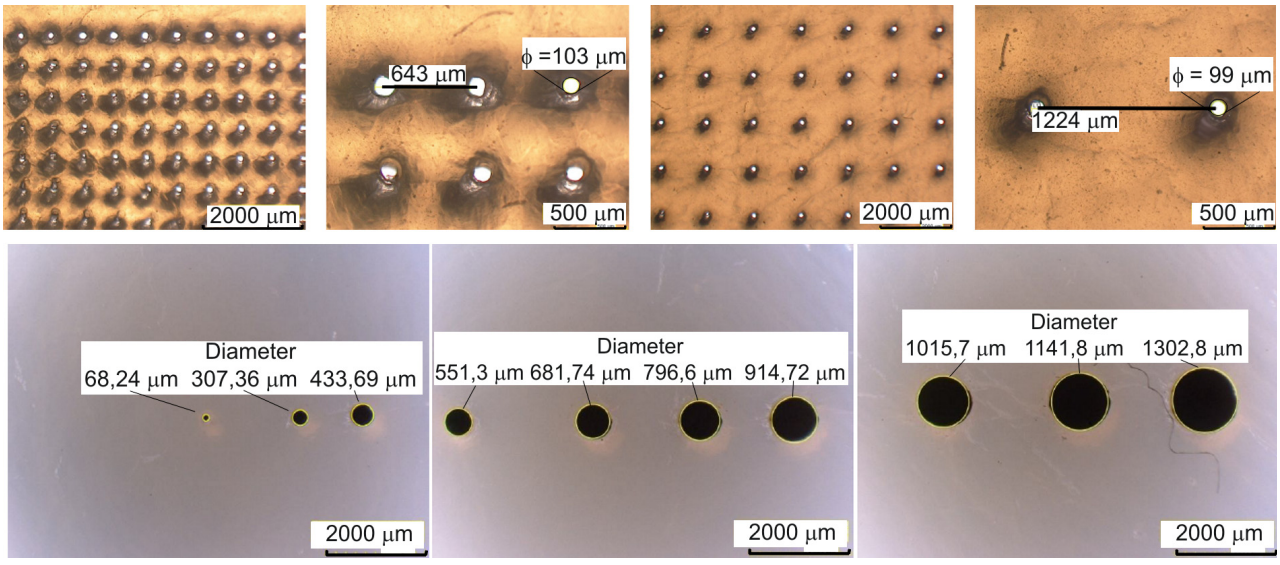

Fig. 10. Illustration of 1D and 2D CO_2 laser perforation of hydrogels as matrices with different periods and aperture diameters

3.2.1. General notation of "n" laser beam interference

The resultant electric field $\vec{E}$ of many interfering laser beams is obtained through superposition of each individual field $\vec{E}_j$ from each beam. This combined field can be represented as follows:

$$\vec{E} = \sum_{j=1}^{n} \vec{E}_j = \sum_{j=1}^{n} \vec{E}_{j0} \cdot \exp\left[-i\left(\vec{k} \cdot \vec{r} - \omega \cdot t\right)\right] \tag{1}$$

where: $\vec{E}_{j0}$ – initial value of laser beam electric field vector, $\vec{k}$ – wave number vector, $\vec{r}$ – radial coordinate vector, ω – angular frequency of electric field, and t – time.

The intensity of interference field for two laser beams is equal to:

$$I = 4I_0 \cos^2(kx \sin\theta) \tag{2}$$

with the pattern field period:

$$d = \frac{\lambda}{2\sin\theta} \tag{3}$$

where: I – the resultant intensity of laser beam in equation (2), I_0 – the initial intensity of laser beam, θ – half-angle between the interfering laser beams, and λ – laser wavelength.

Geometries and images of lines, dots and dimples created by two, three and four interfering laser beams are shown in figures 11 and 12. It should be noted that due to possible changes in the intensity, polarisation state, the angle between beams and the propagation angle between the beam and the geometrical normal, DLIL provides creation of almost every desired periodic structure.

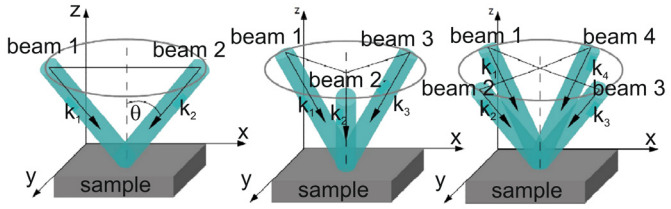

Fig. 11. Representation of an electromagnetic wave in 1D, 2D and 3D configuration. The sample is located at z = 0, i.e. in x,y plane

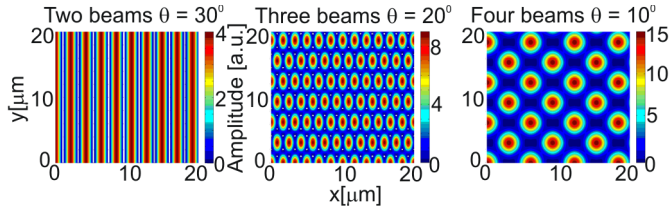

Fig. 12. Calculated examples of interference patterns created by multiple, coherent laser beams: left side – two beam interference and linear pattern; centre – three beam interference and dotted pattern; right side – four beam interference – dimpled pattern

3.2.2. Numerical model of multi-beam ablation in direct interference lithography

(Fig. 13) presents the illumination geometry of a 400 nm thick Al layer, deposited on a quartz substrate using the physical vapour deposition (PVD) method. Orange triangles indicate the number of pulses (two or three), situated at a different distance from one another (1900 and 950 nm respectively) that simultaneously illuminate the target surface. These pulses represent two and three interference patterns, created as a result of interference of two laser beams at proper angles. The temporal shape of an illuminating pulse with a 1 nsec full width at half maximum (FWHM) is shown in the upper part of both figures. An incident radiation power density of 5×10^8 W/cm^2 has been assumed for the theoretical model.

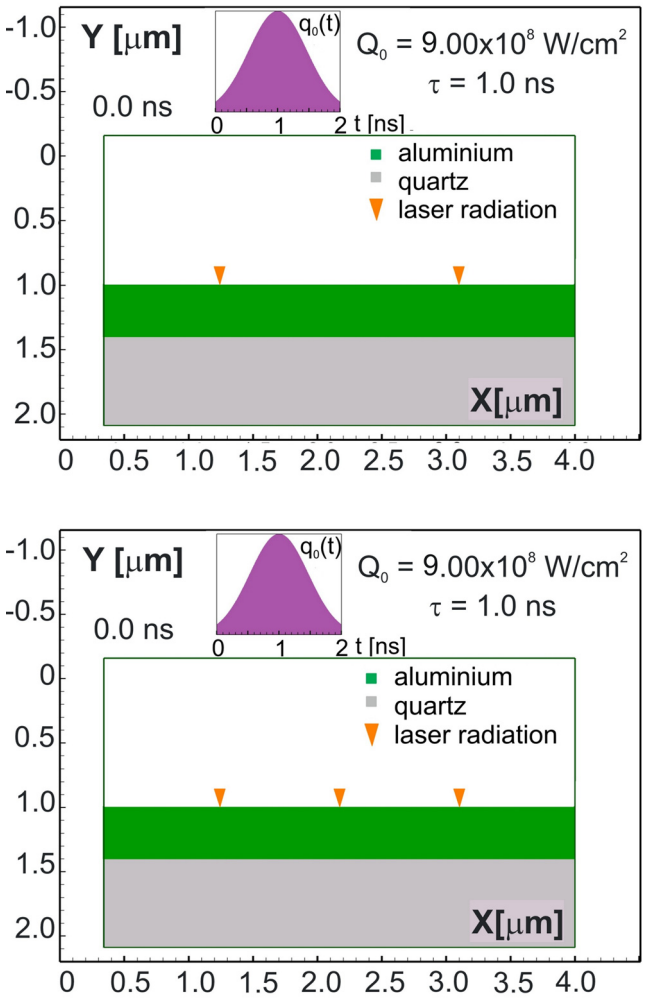

Fig. 13. Geometries of illumination of a 400 nm thick Al layer on a quartz substrate, assumed in the numerical model [23]

The sample results of calculation for two beam interference are shown in figure 14. The length of arrows depicts the values of material ablation velocity of the target. (Fig. 14a) shows the beginning of ablation process after approx. 0.5 nsec, while (Fig. 14b) presents the top of the laser pulse. (Fig. 14c) depicts the end of the laser pulse and (Fig. 14d) shows the further material ablation process of the target, which is continued even after the end of laser pulse (after 3 nsec).

An almost total evaporation of Al layer under the interference field of three patterns can be seen in (Fig. 15b). In the case of two patterns (Fig. 15a) which are located twice as far apart as in the case of a three beam interference, full evaporation of the Al layer down to the substrate is evident and a clear border between the evaporated and unaffected parts of the layer can be seen. It clearly illustrates the need of precise selection of power density of the interfering beams. It should be also noted that numerical calculations indicate a substantial influence of the material physical properties on the quality of generated periodic structures.

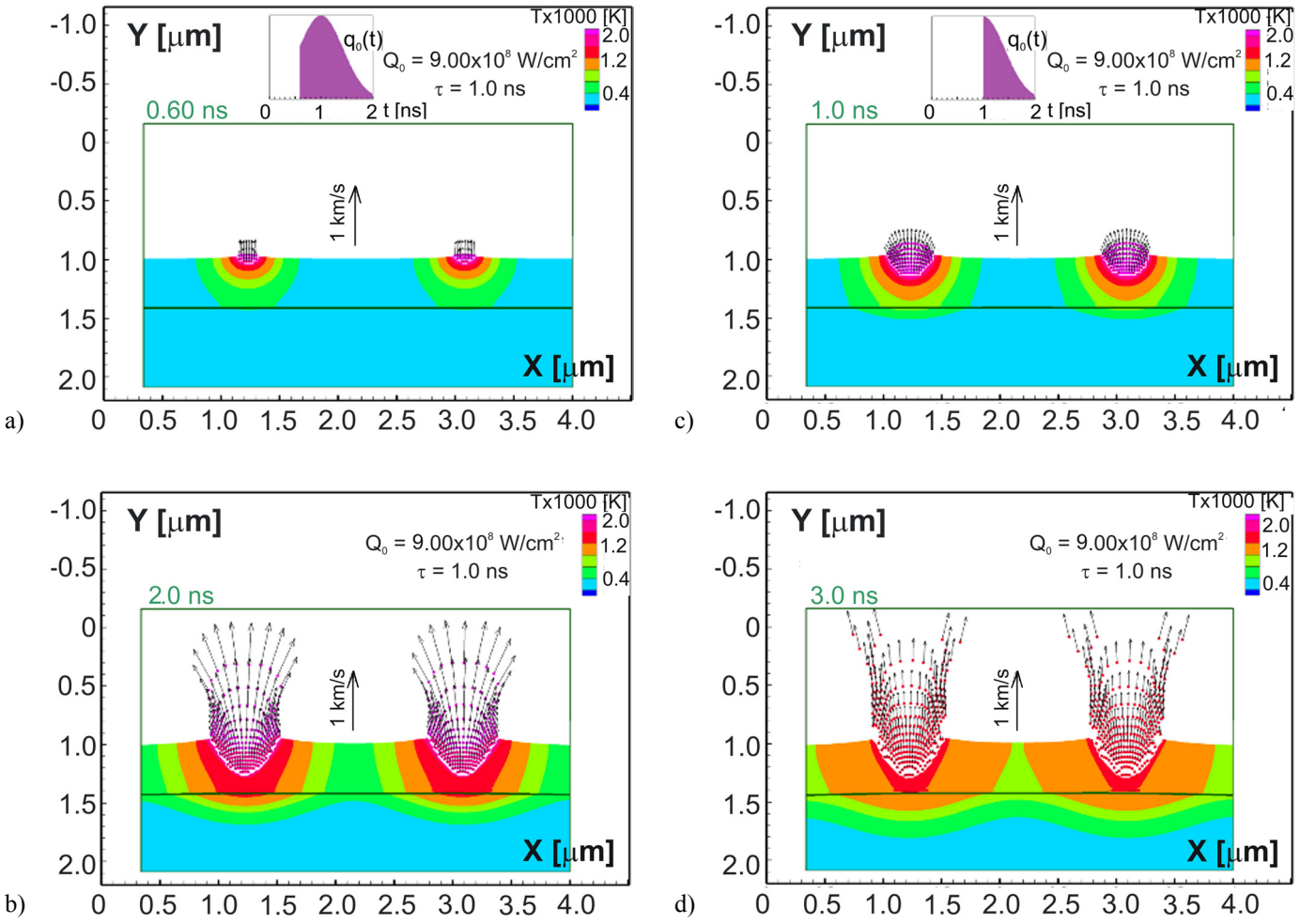

Fig. 14. Selected results of calculations (intermediate stages) for simultaneous interaction of two laser pulses (interference patterns) in subsequent points in time [23]

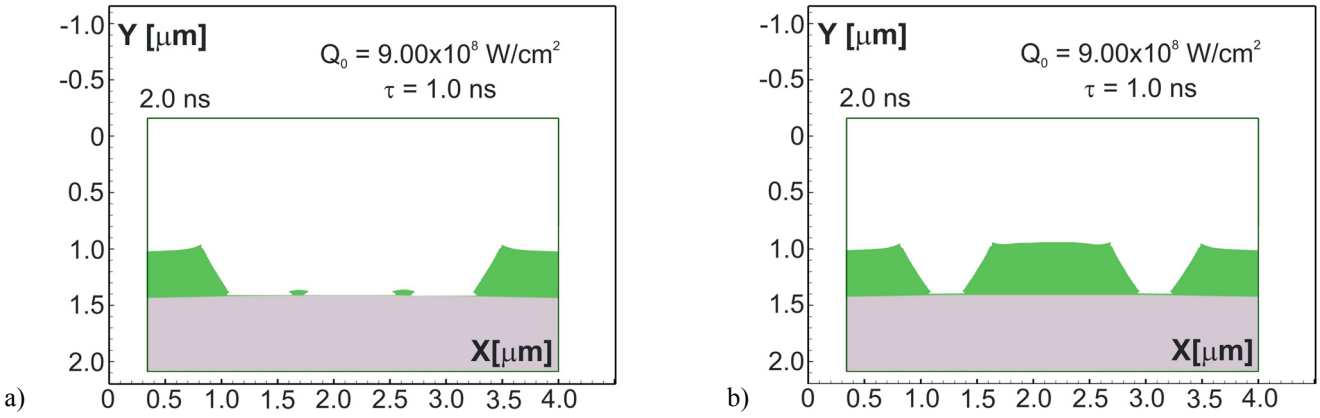

Fig. 15. Results of calculations for craters, created in a 400 nm thick Al layer after the end of a laser pulse for: a) three adjacent patterns of interfering beams; b) two neighbouring patters of interfering laser beams. Laser pulse power density $9 \cdot 10^8$ W/cm^2 [23].

3.2.3. Laser system and dual-beam interferometer

A dual-channel Nd:YAG laser system has been built for direct interference lithography with the pulse energy from one channel of approximately 1.5 J and repetition up to 10 Hz (Fig. 16). The Nd:YAG laser oscillator with Q – modulation operated in a "p – branch" type unstable resonator. The output of the laser beam was realised through a quarter-wave plate and a dielectric polariser, and a diaphragm placed inside the resonator provided a basic transverse mode. Splitting into two energetically equal laser beams on a dielectric mirror occurred at the generator output. Both laser beams were directed into two

channels with two amplifiers in each of them [24,25]. The next step consists of shaping and combining of two laser beams with quasi-planar wave fronts, emitted from the dual-channel laser, inside a Mach-Zehnder interferometer. In consequence, this simple system configuration allowed, after superimposing the output beams at appropriate angles, for fast creation of a periodic structure on the surface with dimensions of several cm^2. The basic system generated an amplified fundamental wavelength of 1064 nm from the Nd:YAG pulse oscillator. The second and third harmonics, 532 and 355 nm respectively, were obtained from an integrated system of frequency converters, which is also shown in (Fig. 16).

One main advantage of the laser system from (Fig. 16) is the possibility to easily change the depth and width of the interference traces as a result of independent laser pulse gain control in the final amplifying channels.

Similar to other interferometric systems, superposition of laser beams at different angles allows creation of hierarchical structures, characterised by variation of the period and/or the dimensions of fabricated structures. It should be noted that creation of hierarchically shaped surfaces poses a major challenge, particularly due to the dependence of the final structure quality on the laser energy density in each subsequent step (each type of grid).

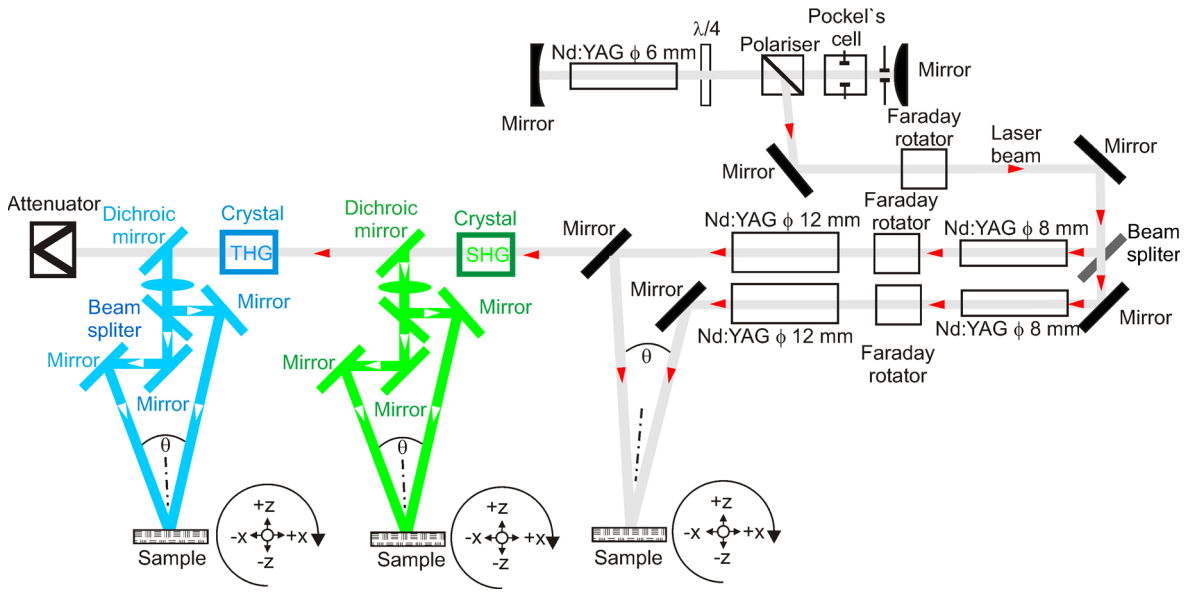

Fig. 16. Experimental setup for direct interference lithography, generating fundamental Nd:YAG laser wavelength and its II and III harmonics [24]

3.2.4. Selected experimental results of modification of material surface layers

Cu/Cr films on quartz substrate

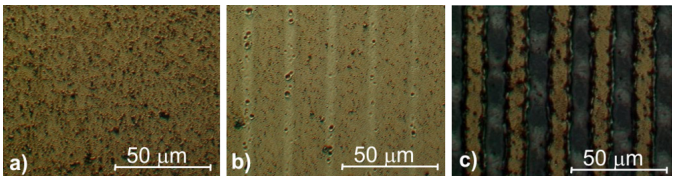

Fig. 17. Topography of Au surface as a function of energy density F (fluence): a) $F < F_{vaporisation}$ lack of surface structuring; b) $F_{vaporisation} < F < F_{ablation\ threshold.}$, structuring without material removal – surface polishing; c) $F_{ablation\ threshold} < F$, structuring with material removal (ablation of gold layer)

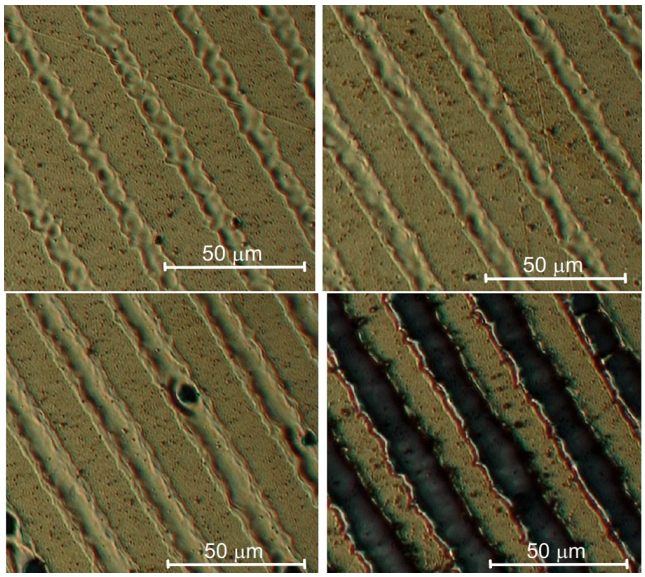

Fig. 18. Examples of maintaining a constant period of diffraction grating with changes in the depth and width of the created hollows. Structuring, similar to the example from figure 17, has been performed on a 50 nm thick Au layer underlain by a 20 nm thick Cr layer. Both metal films were deposited on a quartz substrate using PVD method

Ti6Al4V alloy

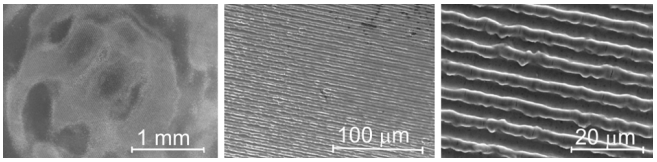

Fig. 19. SEM images of a periodic structure engraved into Ti6Al4V alloy surface, shown in different magnifications. Laser wavelength 1064 nm, energy density above the ablation threshold

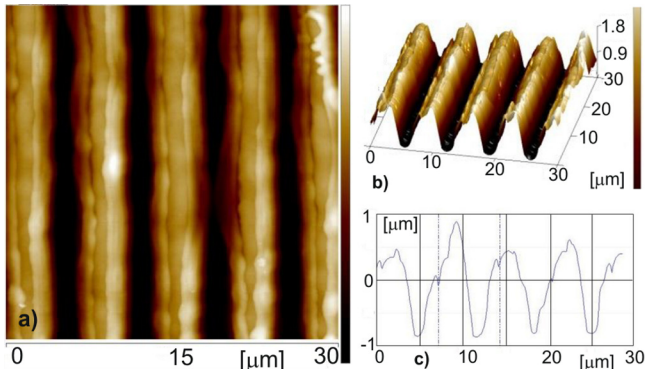

Fig. 20. AFM height profile (a), 3D profile (b) and cross section analysis (c) of the periodic structure from (Fig. 19c)

Ti13Nb13Zr alloy

Literature describes studies on conventional laser remelting of Ti6Al4V and Ti13Nb13Zr alloy surfaces before the process of deposition of hydroxyapatite (HAp) layers [26]. It has been assumed that laser interference micromachining will cause more regular roughness distribution over the alloy surface, along with high control of the period, height and thickness of the created pattern grids. Such preparation of titanium surface can improve the wettability and ordering of deposited HAp layers. Moreover, this in turn enables decreasing HAp film thicknesses and improving their adhesion to the Ti13Nb13Zr alloy surface. These assumptions have been confirmed during preliminary experiments with the use of DLIL technology [27]. One of the results of DLIL structuring is shown in (Fig. 21). It can be seen that the structure of deposited HAp layer partially mimics the linear structure of the substrate interference pattern.

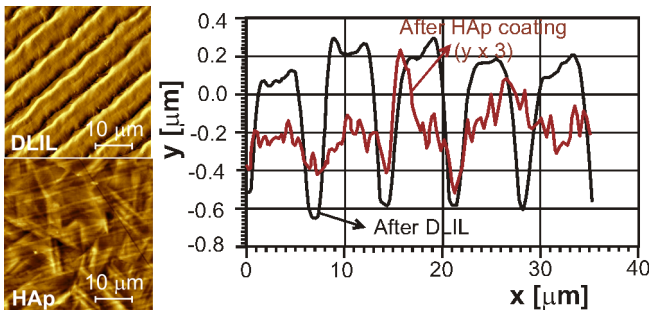

Fig. 21. AFM photomicrographs and profiles of Ti13Nb13Zr bioalloy surface after direct laser interference lithography (DLIL) and subsequent hydroxyapatite (HAp) electrophoretic coating. Laser energy 2×430 mJ (one shot), wavelength 1064 nm.

Moreover, it has been stated after several measurement cycles that: HAp roughness increased 3 times in comparison with roughness on the ground surface; the hardness of HAp layer was higher (10.1 GPa) than of the bioalloy itself (3.7 GPa); and that HAp layer adhesion was continuously growing with the increase in laser pulse energies (nanoscratch test).

DLC layer on a polystyrene substrate

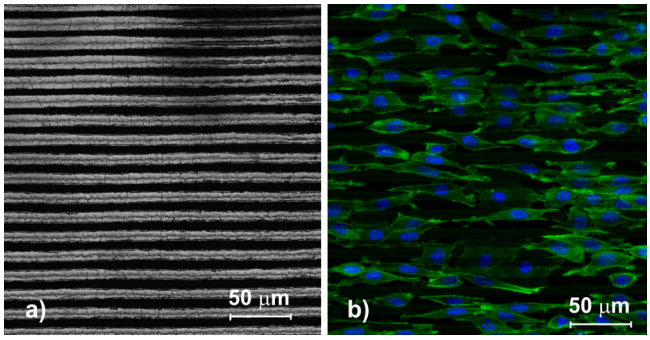

Fig. 22. a) Optical microscope image of a linear structure shaped as patterns illuminated using II harmonics of Nd:YAG laser. DLC thickness on a polystyrene substrate was 300 nm; b) Confocal microscope image of smooth muscle cells grown on a structure from (a) [28]. The cell cultivation method has been described elsewhere [29]

3.3. Self-organised Laser Induced Periodic Surface Structures (LIPSS)

Instabilities, which are observed during laser machining, are connected to a positive feedback between the laser beam and the surface of the treated material. The appearance of instabilities means that an initially small perturbation is increased and amplified during the course of the process. Further development of instabilities can lead to various self-organising phenomena. One of these phenomena, the spontaneous creation of a laser induced periodical surface structure (LIPSS), colloquially named "ripples" [30-32], is described below.

Such kinds of structures, created on solid surfaces under the impact of laser light, are classified as coherent (resonant) and incoherent (non-resonant) structures. Coherent structures are connected to the coherence of laser beam, wavelength and polarisation of laser radiation. They have a common source, namely the oscillating radiation field on the material surface that is generated by the interference between the incident laser beam and the scattered surface waves. Spatial periods of those structures are basically proportional to the wavelength of laser radiation (Fig. 23a). In the case of incoherent structures, they are not connected to the coherence and wavelength (Fig. 23b).

The first, widely accepted, descriptive LIPSS theory assumes that these structures emerge as a result of the interference of the incident laser beam with scattered electromagnetic waves, created at the surface irregularities – its roughness [30]. (Fig. 24) illustrates scattering of the planar wave $\vec{k}_i$, incident at angle θ_{inc} in the direction of one of the spatial frequency components k_{rough} of surface irregularities.

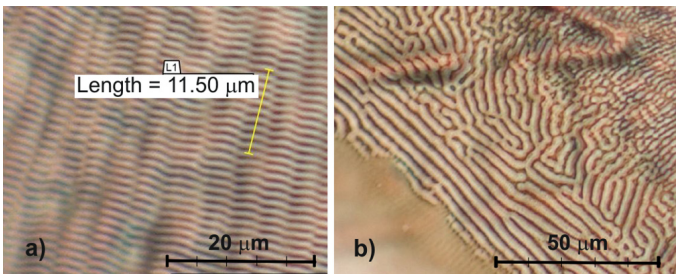

Fig. 23. Optical microscope images of two periods of "ripples": a) individual (~λ), created inside the illumination area of FeSiB amorphous foil, below melting point, with the use of a series of about 10^4 pulses with the duration of 60 ps, the energy of 3 mJ and the pulse repetition rate of 1 kHz; b) with multiple wavelengths, obtained after illumination of FeSiB amorphous foil by a Q-switched Nd:YAG laser beam (nanosecond pulses), just beneath the melting point [30]. Clearly visible is the change of linear structure into a more complex two-dimensional area.

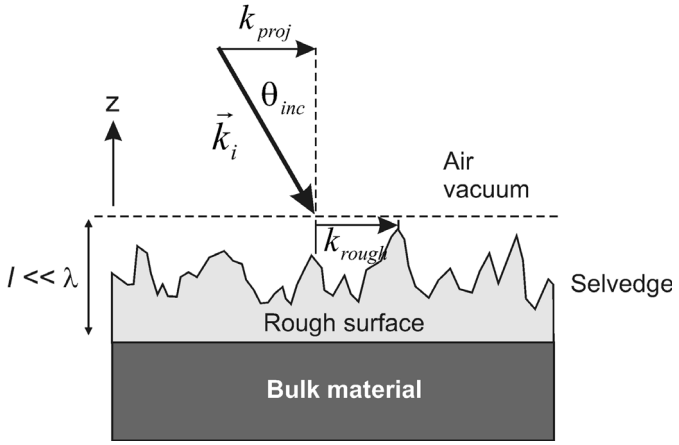

Fig. 24. The geometry of light incident on a rough surface

The abovementioned theory generally correctly describes the identical (in some measure homogeneous) distribution of the interference image with periodical dependence on laser wavelength and the angle of incidence against target surface. These fine "ripples" are positioned perpendicularly to the direction of laser light polarisation, and the period of the resulting ripples depends on laser radiation wavelength, the reflection coefficient of the illuminated target material as well as on the angle of incidence of laser beam with respect to the illuminated surface. The distance d between the ripples changes with the angle of incidence of laser beam θ with respect to the normal to the surface. The dependence of period d during reflection of the beam polarised in the plane "p" ("π") is expressed by:

$$d^{(p)} = \frac{\lambda}{1 \pm \sin\theta} \tag{4}$$

and, in the case of refraction, by:

$$d^{(p)} = \frac{\lambda}{n \pm \sin\theta} \tag{5}$$

where n is the refraction coefficient of the illuminated material and the plus or minus signs relate, respectively, to the direction of surface waves, running towards or away from the inclined surface. In most cases, the direction of ripples is perpendicular to the electric field vector (polarisation) of the incident laser beam. Other dependence describes the ripple period for "s" ("σ") polarisation of the laser beam, namely:

$$d^{(S)} = \frac{\lambda}{\cos\theta} \tag{6}$$

and in the case of refraction:

$$d^{(S)} = \frac{\lambda}{n\cos\theta} \tag{7}$$

Scattering of the incident light is caused by microscopic surface roughness, defects or spatial changes in the dielectric constant. The interference between different wavelengths of the scattered waves leads to heterogeneous energy absorption in the material electron system, which, jointly with the positive feedback mechanism, creates the periodic structures. The intensity of scattered waves depends on the parameters of laser beam and on the type of material. It is assumed that scattered light can directly excite the surface electromagnetic wave (SEW) only if the material possesses an optically active mode close to the laser frequency. Such SEW or surface plasmon polariton (SPP) is a wave which travels along a metal-dielectric or metal-air interface.

The period of "ripples" depends on laser fluence, the number of pulses, the wavelength, the angle of incidence as well as on the laser beam polarisation (Fig. 25). LIPSS have been observed for almost half a century [33] and still there is little clarity about the mechanism that plays the dominant role in many experiments described in literature, particularly those that utilise femtosecond pulses [32].

(Fig. 26) presents a previously unpublished microphotograph, which according to the Author's knowledge is the first experimental proof of perpendicular LIPSS arrangement with respect to the electric field vector of laser radiation. It can be seen that ripples were created along the direction perpendicular to the interference patterns, which were obtained using simultaneously direct interference lithography on the Al layer, deposited onto a quartz substrate.

Creation of ripples can be utilised in fabrication of grids for well-defined orientation of molecules, directional growth of biological cells etc. Combination of different structuring techniques (e.g. DLW+DLIL+ripples) opens an enormous diversity of possibilities. Periodical sub-micron grids and dotted structures, generated by simultaneous creation of ripples and laser interference patterns are only some of the representative examples among many, many others.

3.4. Combined methods

Quartz glass is a very poor absorber of light, starting from the deep ultraviolet (UV) to the near infrared (IR) region of light radiation. Precise engraving of micro/nano structures into quartz surface using laser ablation requires accordingly high peak power densities, above GW/cm^2. That is why ablative structuring of quartz surface is realised in vacuum, with the use of UV lasers,

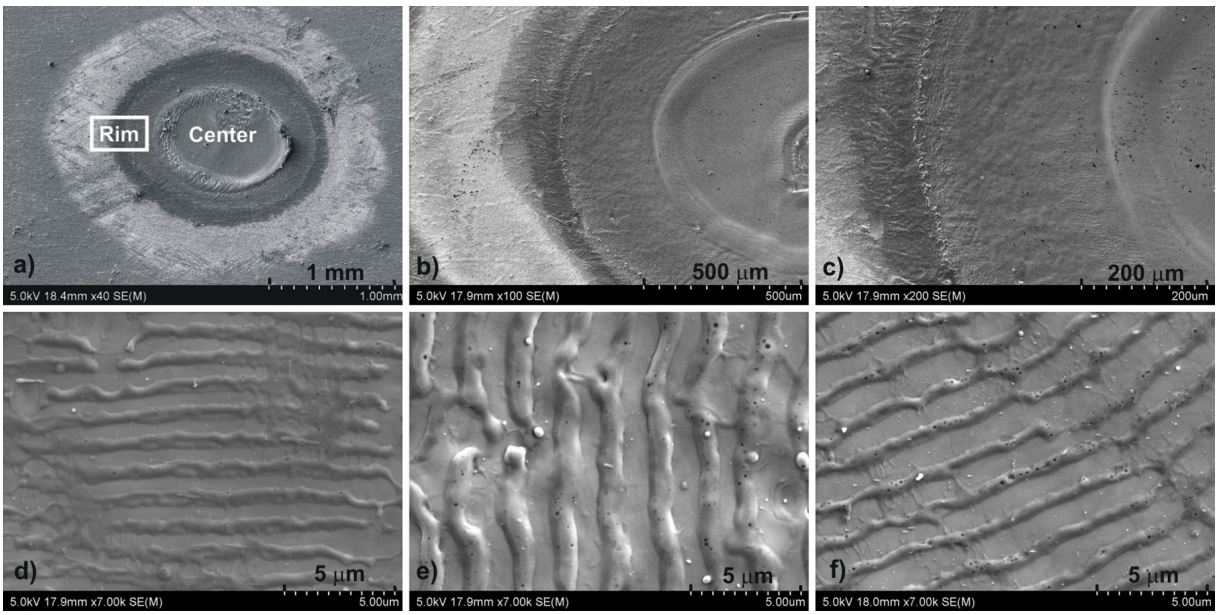

Fig. 25. a-c) Subsequent SEM magnifications of areas of "ripple" generation; d-f) SEM images of "ripples" for different beam polarisation: d) "p"– polarisation; e) "s" – polarisation; f) circular polarisation. Fe-Si-B amorphous foil, 100 laser shots, laser fluence 0.74 J/cm^2 [34]

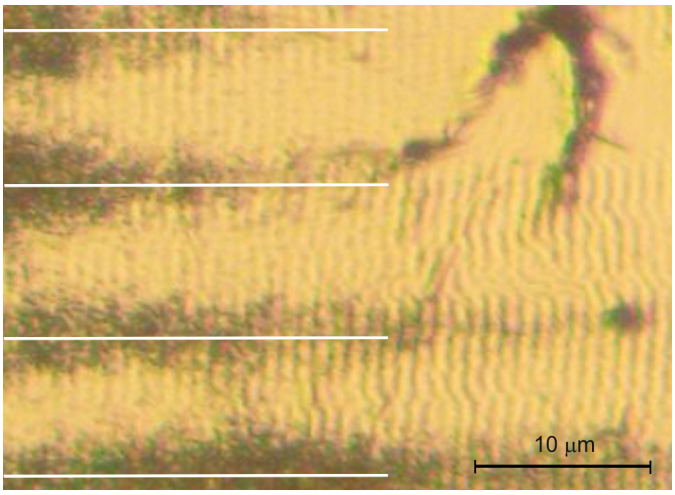

Fig. 26. Experimental proof of creation of "ripples" perpendicular to the electric field vector of laser radiation, which is indicated by white lines in the centres of linear interference patterns

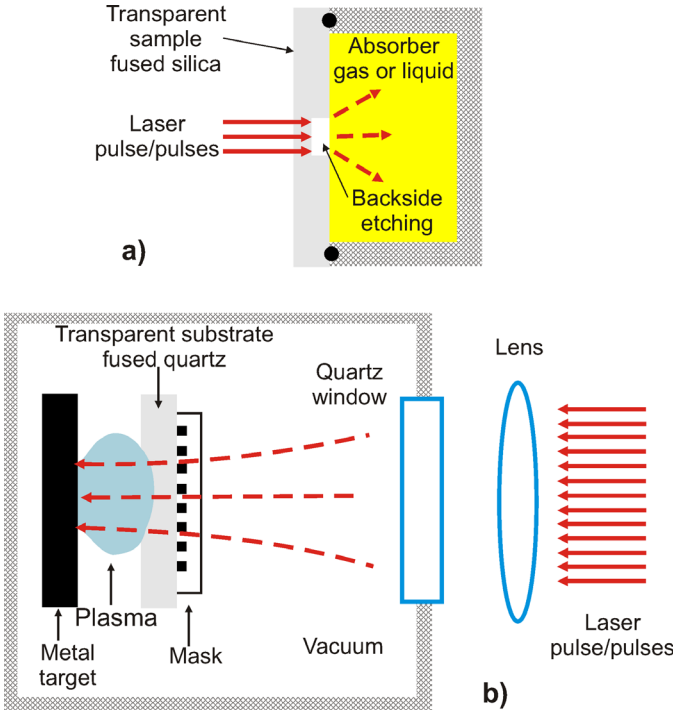

Fig. 27. Depiction of indirect ablation methods: a) Laser Induced Backside Wet or Dry Etching (LIBW/DE); b). Laser Induced Plasma Assisted Ablation (LIPAA)

e.g. 157 nm and 193 nm excimer lasers [35] or femtosecond lasers [36], which induce processes of multiphoton absorption. Apart from these direct ablation methods, indirect techniques are applied with the use of external absorbers. Among the direct methods of ablation of e.g. quartz surfaces, the following are distinguished:

– laser induced backside wet etching (LIBWE), (Fig. 24a) [37,38];
– laser induced plasma assisted ablation (LIPAA), (Fig. 24b) [39];

Derived from those indirect methods presented in (Fig. 27) are the following techniques:

– laser induced backside dry etching (LIBDE), shown in (Fig. 28a);
– laser induced frontside dry etching (LIFDE), shown in (Fig. 28b).

All these ablation processes relate to the etching of back surface, which means that laser beam should first travel through the treated sample before inducing ablation of the back side where the absorber is located. The limitation of this method is the need of a flat front side of the sample.

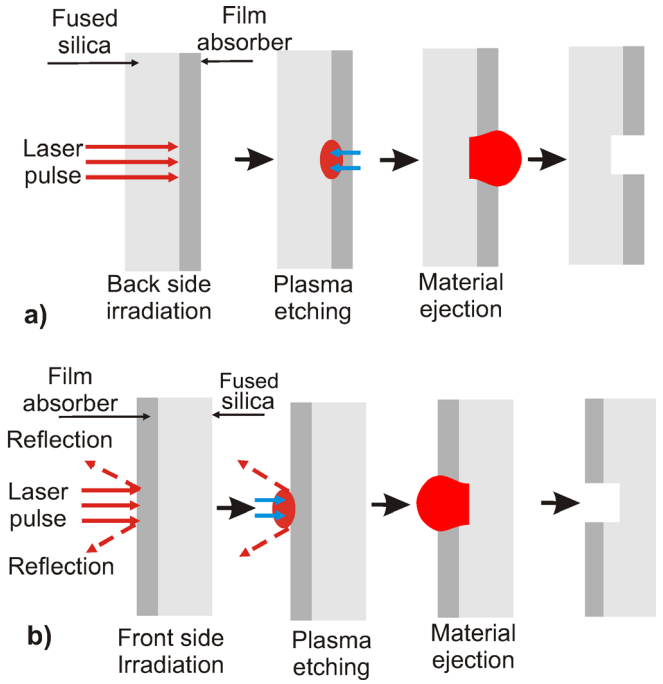

Fig. 28. Optical chart of backside (a) and frontside (b) configuration for laser etching of transparent materials, using e.g. thin metal film absorbers

The ablation method shown in (Fig. 27a) is utilised in compressive experiments (e.g. laser shock peening, laser fusion) and involves focusing the laser beam on an opaque removable layer positioned on a transparent substrate made of a different material. The absorbed energy is transferred mainly to the internal energy of the target material, while the kinetic energy constitutes only its minimal part. The transparent layer acts as a target-buffer which prevents the expansion of material in the direction opposite to the incident laser beam. The pressure, created at the interface between quartz and the absorbing metal film, induces expansion of material in the direction of laser beam incidence (propagation). The thin film of opaque material (chromium and gold layer in (Fig. 28a) is removed from the back substrate surface under the impact of the laser beam, creating a periodic structure. The next advantage of this method results from the decrease of the required fluence compared to the method shown in (Fig. 28b).

(Fig. 29) illustrates the use of LIBDE method in fabrication of diffraction grating on the surface of fused quartz. Fused quartz sample was coated with thin films of chromium and gold (PVD deposition, 20 nm Cr and 50 nm Au). Illumination of the sample from the side of quartz with two interfering Nd:YAG laser beams resulted in creation of interference patterns inside a diameter of 10 mm (Fig. 29b).

Microscopic images of the results of the LIBDE process after chemical treatment of structures are shown in (Fig. 30). An interesting effect is the image of Au and Cr nano-strips which were delaminated during etching. Figure 31 in turn presents the results of a SEM EDS analysis of the chemical composition of the resulting linear pattern grid, which confirms a precise, complete ablation of the Au+Cr layer in the bright areas of the periodic structure.

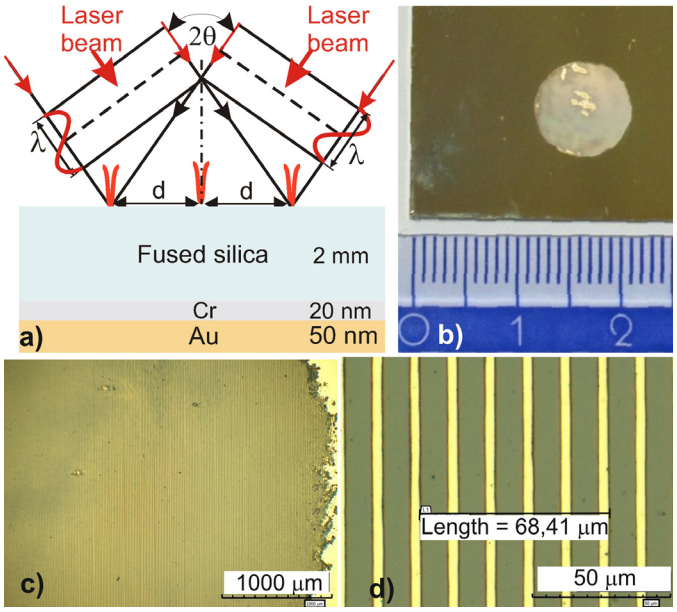

Fig. 29. Fabrication of diffraction grating on the surface of fused quartz: a) Sample illumination geometry; b) View of the pattern area with a diameter of 10 mm; c) Images of a periodic structure at the edge of a spot from an optical microscope; d) strong microscopic magnification of the image from c)

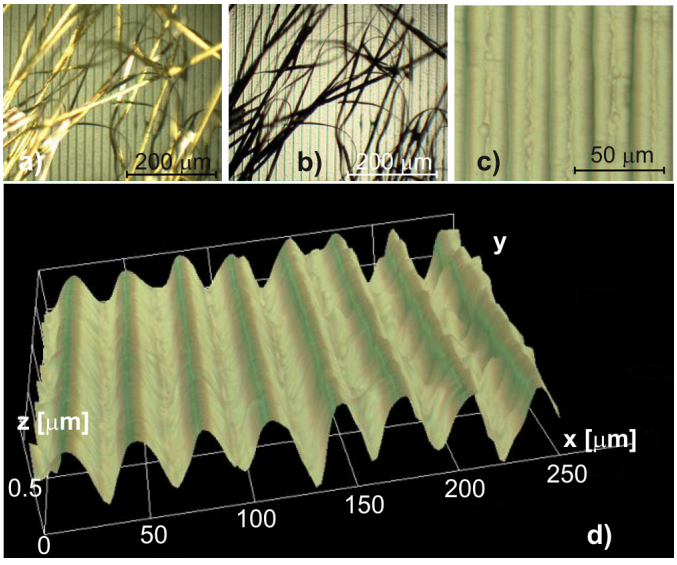

Fig. 30. a-b) Images of Au and Cr nano-strips after chemical treatment, taken from an optical microscope in reflected (a) and transmitted (b) light. The background is an etched microstructure on a quartz substrate; c) Optical microscope image of a quartz substrate after etching in HF acid; d) 3D optical microscopic image of the structure from c)

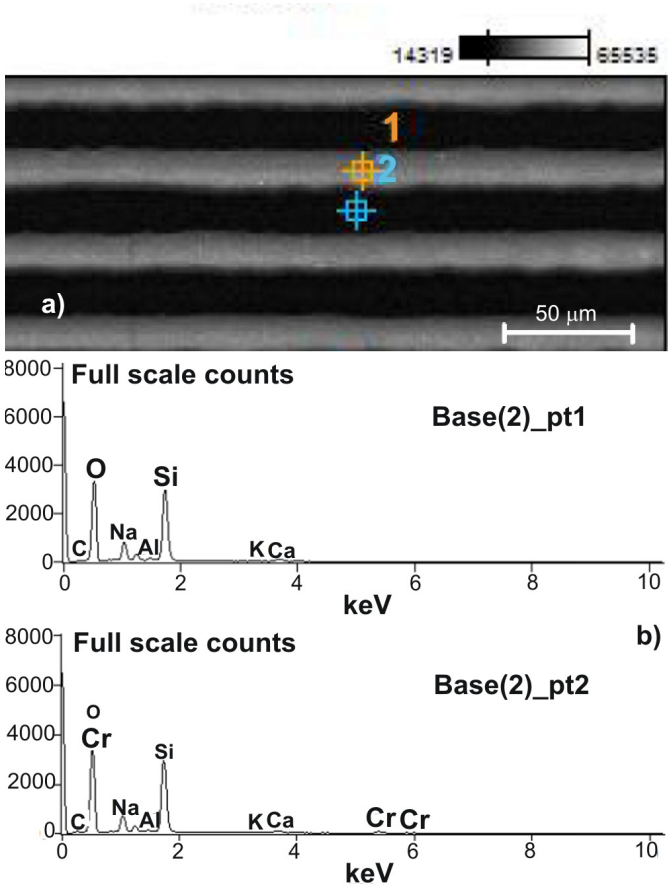

Fig. 31. SEM EDS analysis of the chemical composition of linear patterns from (Fig. 30 a) Fragment of SEM (Z contrast) image; b) Point EDS analysis of quartz surface after etching

4. Summary

Fabrication of periodic structures with micron and submicron features on the surface of different materials is a fast developing field of research, with promising applications in many scientific, technological and medical areas, including bioengineering.

The micromachining process utilises mainly laser ablation, which is a multipurpose tool able to produce 1D-3D structures and to modify the surface or the volume of materials. The ablation process allows treatment of any materials, from the hardest and most refractory to plastic ones. The size, shape, location and density of micro/nano structures depends on a given method of surface modification as well as on the laser wavelength, the pulse duration (also the number of pulses), the energy density (fluence) and the material data. Such reciprocal coupling of parameters (laser and material) assures high precision of treatment (high resolution) and low costs, even during the machining of such transparent materials as quartz or glass.

Maximum benefits result from application of direct interference lithography in the creation of densely packed structures in micro and sub-micro scale within wide areas during one technological process lasting several seconds. The use of two or more interfering light beams from high peak power lasers provides the possibility of direct treatment of the surface of materials (including metals, ceramics and polymers) based on a photothermal and/or photochemical ablation mechanism.

The surfaces modified this way can be used in many areas of applications, starting from tribology (wear reduction) and ending in bioengineering.

Integration of different techniques of laser shaping of solid surfaces enables creation of hierarchical, multilevel and multidimensional changes in topography and microstructure. It will undoubtedly enable significant progress in biomimetics, followed by development in other fields.

REFERENCES

[1] T.H. Maiman, Nature **187**, 493 (1960).
[2] L.J. Radzemski, D.A. Cremers, Laser induced plasmas and applications, Dekker, New York 1989.
[3] M. Allmen, A. Blatter, Laser beam interaction with materials, Second Edition, Springer, Berlin, Germany 1995.
[4] J.F. Ready, D.F. Farson, Handbook of laser materials processing, Magnolia Publishing Inc., Orlando, USA 2001.
[5] B. Major, Chapter 7: Laser processing for surface modification by remelting and alloying of metallic systems, in: Y. Pauleau (Ed.), Materials surface processing by directed energy techniques, Elsevier (2006).
[6] J.M. Lackner, W. Waldhauser, L. Major, J. Morgiel, M. Kot, B. Major, Bull. Pol. Acad. Tech. **54**, 175 (2006).
[7] D. Bauerle, Laser Processing and Chemistry, Fourth Edition, Springer-Verlag Berlin, Heidelberg, New York 2011.
[8] R. Ebner, J.M. Lackner, W. Waldhauser, R. Major, E. Czarnowska, R. Kustosz, P. Lacki, B. Major, Bull. Pol. Acad. Tech. **54**, 167 (2006).
[9] B. Major, F. Bruckert, J.M. Lackner, R. Ebner, R. Kustosz, P. Lacki, Arch. Metal. Mater. **53**, 39 (2008)
[10] B. Major, R. Major, F. Bruckert, J.M. Lackner, R. Ebner, R. Kustosz, P. Lacki, Adv. Mater. Sci. **7**, 63 (2007)
[11] J. Kusiński, S. Kąc, A. Radziszewska, M. Rozmus-Górnikowska, B. Major, R. Major, J. Marczak, A. Lisiecki, Bull. Pol. Acad. Tech. **60**, 711 (2012).
[12] J.C. Miller, Laser ablation: Principles and Application, Springer Series in Mater. Sci. **28** (1994).
[13] J. Marczak, Proc. SPIE **4402**, 202 (2001).
[14] M. Strzelec, J. Marczak, D. Chmielewska, A. Sarzyński, A. Olszyna, K. Szamałek, D. Zasada, Photonics Letts Poland **5**, 134 (2013).
[15] W.M. Steen, J. Mazumder, Laser Material Processing, 4th Edition, Springer, London, Heidelberg, New York 2010.
[16] B. Furlong, S. Motakef, Photonik International, **3**, 20 (2008).
[17] R. Major, K. Maksymow, J. Marczak, J.M. Lackner, M. Kot, and B. Major, Bull. Pol. Acad. Tech. **60**, 337 (2012)
[18] C.G.K. Malek, Anal. Bioanal. Chem. **385**, 1362 (2006).
[19] B.H. Weigl, R.L. Bardell, N. Kesler, C.J. Morris, Fresen. Z. Anal. Chem. **371**, 97 (2001).

[20] O. Sarig-Nadir, N. Livnat, R. Zajdman, S. Shoham, D. Seliktar, Biophys. J. **96**, 4743 (2009).
[21] S. Aisenberg, R. Chabott, J. Appl. Phys. **42**, 2953, (1971).
[22] J. Robertson, Diamond-like carbon, Pure Appl. Chem. **66**, 1789 (1994).
[23] J. Marczak, K. Jach, R. Świerczyński, M. Strzelec, Int. J. Latest Res. Sci. Techn. **2**, 18 (2013).
[24] J. Marczak, A. Rycyk, A. Sarzyński, M. Strzelec, J. Kusiński, R. Major, Proc. SPIE **8703**, 87030F (2013).
[25] J. Marczak, A. Rycyk, A. Sarzyński, M. Strzelec, K. Czyż, Photonics Letts Poland **6**, 44 (2014).
[26] A. Zieliński, S. Sobieszczyk, W. Serbiński, T. Seramak, A. Ossowska, Solid State Phenom. **183**, 225 (2012).
[27] B. Majkowska, M. Jazdzewska, A. Zielinski, J. Marczak, A. Sarzyński, M. Strzelec, A. Rycyk, K. Czyż, EMRS Fall Meeting 2014, Poster Session R2: http://www.emrs-strasbourg.com/index.php?option=com_abstract&task=view&id=284&year=2014&Itemid=&id_season=12&PHPSESSID=633883b1743e9ddf607fee432898b962.
[28] R. Major, F. Bruckert, J. Marczak, J.M. Lackner, J. Marczak, B. Major, RSC Advances **4**, 9491 (2014).
[29] J. Marczak, J. Kusiński, R. Major, A. Rycyk, A. Sarzyński, M. Strzelec, K. Czyż, Opt. Appl. **44**, 575 (2014).
[30] J.E. Sipe, J.F.Young, J.S. Preston, H.M. van Driel, Phys. Rev. B. **27**, 1141 (1983).
[31] H.M. van Driel, J.E. Sipe, J.F. Young, J. Luminesc. **30**, 446 (1985).
[32] G.R.B.E. Römer, A.J. Huis in't Veld, J. Meijer, M.N.W. Groenendijk, CIRP Ann-Manuf. Techn. **58**, 201 (2009).
[33] M. Birnbaum, J. Appl. Phys. **36**, 3688 (1965).
[34] J. Marczak, K. Czyż, J. Kusiński, T. Onyszczuk, A. Rycyk, A. Sarzyński, M. Strzelec, Materials Engineering **35**, 523 (2014). In Polish.
[35] J. Ihlemann, B. Wolff, P. Simon, Appl. Phys. A **54**, 363 (1992).
[36] J. Krüger, W. Kautek, Appl. Surf. Sci. **96-98**, 430 (1996).
[37] R. Böhme, K. Zimmer, B. Rauschenbach, Appl. Phys. A **82**, 325 (2006).
[38] P. Lorenz, M. Ehrhardt, A. Wehrmann, K. Zimmer, Appl. Surf. Sci. **258**, 9138 (2012).
[39] Jie Zhang, Koji Sugioka, Katsumi Midorikawa, Opt. Lett. **23**, 1486 (1998).

Received: 20 April 2015